Petroleum Science 23 (2026) 4183–4192

Contents lists available at ScienceDirect

Petroleum Science

journal homepage: www.keaipublishing.com/en/journals/petroleum-science

Original Paper

Thickening characteristics and conformance control mechanism of CO_2-responsive fluid during CO_2 flooding

Xiao-Guang Wang [a,b], De-Hua Liu [a], Hong-Bin Cheng [c], Qiang Luo [b], Ke Tang [b], Dao-Yi Zhu [c,*]

[a] School of Petroleum Engineering, Yangtze University, Wuhan, 430100, Hubei, China
[b] Research Institute of Petroleum Exploration and Development, Xinjiang Oilfield Company, PetroChina, Karamay, 834000, Xinjiang, China
[c] School of Petroleum, China University of Petroleum-Beijing at Karamay, Karamay, 834000, Xinjiang, China

ARTICLE INFO

Article history:
Received 23 January 2026
Received in revised form
19 March 2026
Accepted 19 March 2026
Available online 23 March 2026

Edited by Yan-Hua Sun

Keywords:
CO_2 responsive fluid
Thickening mechanism
Heterogeneous reservoir
Channeling control
Nuclear magnetic resonance

ABSTRACT

CO_2-responsive fluid (CRF) is a surfactant solution characterized by low viscosity during the injection stage, and by a viscosity increase after reaction with CO_2, which achieves mitigation of CO_2 channeling. CRF has been applied in several pilot tests for CO_2 conformance control in the Xinjiang Oilfield, China. However, its thickening characteristics (i.e., the viscosity change behavior) are not clearly defined, and the mechanism of conformance control requires further understanding. In this study, the static thickening behavior and reservoir adaptability (e.g., reservoir temperature and formation water salinity) of CRF were investigated through viscosity evaluation and microscopic characterization methods. Combining core displacement experiments and nuclear magnetic resonance (NMR) analysis, the CO_2 conformance improvement of CRF in heterogeneous cores was examined. Results indicated that the viscosity of CRF after reacting with CO_2 increased with the concentrations of reagent A (tertiary-amine single-chain surfactants) and reagent B (quaternary ammonium gemini surfactants), reaching a maximum of 460 mPa·s with the optimal composition of 1.5% reagent A and 0.2% reagent B. A mathematical equation for static thickening behavior was established to predict viscosity variation, providing a basis for rapid screening before oilfield applications. FTIR analysis confirmed that tertiary amine groups in the CRF molecular structure possessing CO_2-responsive functionality, as thickening occurred through protonation reaction. SEM observation showed that CRF exhibited a lamellar morphology before reaction with CO_2, while three-dimensional (3D) network structures formed after reaction due to micelle formation. NMR T_2 spectra demonstrated that CRF had significant plugging and CO_2 conformance control effects in the three-layer heterogeneous core with the permeabilities of 100/300/1500 $\times$ 10^{-3} μm^2, effectively delaying CO_2 channeling. This study provided CO_2-responsive thickening systems and technical guidance for further development and field-scale application of CRF for conformance control during CO_2-EOR processes.

1. Introduction

CO_2 enhanced oil recovery (CO_2-EOR), as an essential component of the integrated technology for enhanced oil recovery (EOR) and carbon capture and storage (CCS), has received extensive global attention in recent years (Chen et al., 2022; Yan et al., 2026; Zhu, 2023). By injecting CO_2 into the reservoir, crude oil viscosity can be effectively reduced, and fluidity can be improved. Meanwhile, CO_2 can be permanently stored in the formation while increasing oil production, achieving the dual goals of emission reduction and production enhancement (Li et al., 2023; Lv et al., 2022; Zhang et al., 2024). Particularly in mature and low-permeability reservoirs, CO_2 flooding exhibits significant economic and environmental benefits during secondary and tertiary oil recovery stages (Chen et al., 2023a; Huang et al., 2024a). However, severe gas channeling often occurs in heterogeneous reservoirs during CO_2 flooding, which limits the sweep volume and reduces oil recovery (Wang et al., 2023; Zhao et al., 2022). Therefore, how to maintain efficient CO_2 flooding while improving conformance and enhancing of

* Corresponding author.
E-mail address: chutaoi@163.com (D.-Y. Zhu).
Peer review under the responsibility of China University of Petroleum (Beijing).

https://doi.org/10.1016/j.petsci.2026.03.043

CO_2 sequestration has become a key scientific and engineering challenge (Wu et al., 2025; Zhu et al., 2021).

To address the insufficiency of conformance during CO_2 flooding, various strategies have been developed worldwide, including water-alternating-gas (WAG) injection, CO_2 foam flooding, and polymer-gel plugging methods (Zhu et al., 2021, 2025b). WAG injection methods can reduce gas channeling to some extent, but its strong corrosivity and limited plugging efficiency in high-permeability channels restrict its application (Fang et al., 2025a; Zhu et al., 2025c). CO_2 foam flooding can increase CO_2 viscosity and decrease the mobility ratio. However, foam systems usually exhibit poor stability and limited channeling-control performance under high-temperature and high-salinity conditions (Bai et al., 2025). Polymer-gel systems provide strong plugging capability, yet the high viscosity and poor mobility of in situ crosslinked polymer gels (ISCPG) lead to poor injectivity and operational difficulties, making large-scale application in in-depth reservoirs challenging (Afolabi et al., 2025; Chen et al., 2023b; Sun et al., 2021; Zhu et al., 2026). In contrast, CRFs possess low viscosity and high mobility close to that of water during the injection stage, enabling deeper penetration into the in-depth reservoir (Gao et al., 2024). After reacting with CO_2 in the reservoir, protonation or structural self-assembly occurs rapidly, resulting in a significant increase in viscosity and the formation of a network structure. Therefore, it achieves in-situ thickening and gas-channeling plugging in the reservoir (Zhu, 2023). In recent years, such intelligent conformance-control fluids have shown great application potential. They combine injectivity and responsiveness in improving the conformance of CO_2 flooding and delaying gas channeling. Therefore, the CRF technology has become an important research direction for integrated EOR and CCS development.

The research on CRFs originates from the field of intelligent fluids and stimuli-responsive materials. The main principle is to introduce functional groups into the molecular or micellar structure of the fluid that can chemically react with CO_2 or self-assemble physically. For example, tertiary amine, quaternary ammonium salt, or carbonate precursors (Deng et al., 2025; Zhou et al., 2025; Zhu et al., 2023). CO_2-responsive polymer (CRP) or *in situ* crosslinked polymer gel (ISCPG) systems commonly adopt protonatable amino or amide structures. Through intermolecular electrostatic interactions and hydrogen bonding, 3D networks can be formed. Therefore, they maintain low viscosity during injection and increase viscosity after reacting with CO_2 (Huang et al., 2024b; Wang et al., 2019). Studies showed that the viscosity enhancement of CO_2-responsive polymers is significant under low salinity conditions, but the structural stability decreases in high-salinity environments. Deng et al. (2025) introduced vinyl silica nanoparticles into the conventional preformed particle gel (PPG) composition to prepare CO_2-responsive preformed particle gels (CR-PPGs). They exhibit high plugging strength under the CO_2 atmosphere. However, due to the large molecular weight of CRP or CR-PPGs, injectivity remained limited, particularly in heterogeneous reservoirs with high permeability contrast, making deep conformance control difficult to achieve.

Compared with CRP, CO_2-responsive surfactants (CRS) exhibit more advantages in terms of injectivity. Their molecules consist of a hydrophilic head and a hydrophobic tail. By introducing reactive groups such as tertiary amines or quaternary ammonium salts at the hydrophilic end, when CO_2 dissolves in the aqueous phase to form carbonic acid or bicarbonate, the reactive groups are protonated. It leads to the intermolecular electrostatic interactions. This transformation converts the micellar structure from linear to a 3D network, thereby significantly increasing the solution viscosity (Chen et al., 2023b; Fu et al., 2025; Luo et al., 2025). Su et al. (2013) reported that sodium octadecyl sulfate and 2-(dimethylamino)ethanol can form wormlike micelles in the presence of CO_2. Fang et al. (2025b) prepared a CO_2-responsive hydrogel (HXB-2) using sodium 2-chloropropionate (CHPW-Na) and propyl dimethyl tertiary amine (EAPKO) at a molar ratio of 1.5:1. After reacting with CO_2, the viscosity increases by 4.53 times. Core displacement experiments showed that the oil recovery increases by 23.53 percentage points after using HXB-2. Shen et al. (2021) screened ten surfactants containing tertiary amino groups and found that *N*,*N*-dimethyl erucamide tertiary amine (DMETA) exhibited the best CO_2-responsive performance. Upon contact with CO_2, DMETA forms wormlike micelles, and the viscosity reaches up to 605,700 mPa·s. The responsive viscosity can be adjusted by changing the CO_2 concentration in the system. They possess strong structural designability, rapid viscosity response, and good temperature and salinity resistance. In recent years, CRS has attracted increasing attention in petroleum engineering research (Afolabi et al., 2025). Reported studies indicate that, during CO_2 displacement experiments on core samples from Well Block 530 of the Xinjiang Oilfield, CRS can effectively delay gas channeling, improve conformance, and provide a stabilizing effect for reservoir CO_2 sequestration (Chen et al., 2023b).

However, the research on CRFs has mainly focused on system synthesis, surfactant design, and basic performance testing. Systematic assessments of their thickening characteristics under actual reservoir conditions (e.g., temperature, salinity, pH, and other factors) are still lacking. Meanwhile, the conformance control mechanism of CRF during CO_2 flooding remains incomplete. In particular, studies of flow behavior and plugging processes in heterogeneous porous media have rarely been visualized or quantitatively investigated. For example, quantitative models describing static thickening behavior are still immature, and predictive design parameters are absent for field implementation. The 3D network morphology and flow-path evolution formed after viscosity enhancement reactions in 3D pore structures still need to be clarified.

In this study, tertiary-amine single-chain surfactants and quaternary ammonium gemini surfactants were selected as CO_2-responsive fluids (CRFs). A multiscale comprehensive investigation was conducted on the thickening performance and CO_2 conformance control mechanism of CRFs. Viscosity evaluations and characterizations by FTIR, SEM, and TG/DSC were performed to systematically analyze the static thickening features of CRFs under varying component, temperature, salinity, and pH value. Core displacement experiments were used to quantitatively evaluate the plugging and CO_2 conformance control of the system in heterogeneous reservoirs. The distribution variation of fluids during displacement were analyzed by NMR T_2 spectra. The results will reveal the microscopic mechanism of the CRF reaction-induced viscosity enhancement and its adaptability to reservoir conditions. The findings will further provide a theoretical basis, methodological reference, and data support for the oilfield optimization and large-scale application of CRFs for CO_2 flooding.

2. Experimental materials and methods

2.1. Experimental materials

Sodium chloride (purity 99.5%), hydrochloric acid (purity 37%), and sodium hydroxide (purity 99%) were purchased from Shanghai Macklin Biochemical Technology Co., Ltd., China. CRF reagents, including reagent A (tertiary-amine single-chain surfactants) and reagent B (quaternary ammonium gemini surfactants), with molecular structures shown in Fig. 1, were made by China University of Petroleum, Beijing. Crude oil (viscosity 7.5 mPa·s, provided by Xinjiang Oilfield, China), formation water (salinity 24,000 mg/L,

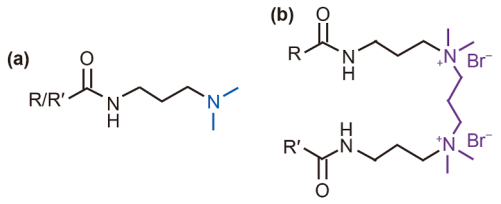

Fig. 1. Molecular structures of CRF reagents. (**a**) Reagent A (tertiary-amine single-chain surfactants); (**b**) reagent B (quaternary ammonium gemini surfactants).

$NaHCO_3$ type, provided by Xinjiang Oilfield), CO_2 (purity 99.9%, supplied by Zhongke Gas Co., Ltd., Karamay, China), and deionized water (prepared in the laboratory) were also used.

The core samples were three-layer heterogeneous artificial sandstone cores, with a length of 6.98 cm and a diameter of 2.50 cm. The three layers had permeabilities of 100×10^{-3}, 300×10^{-3}, and 1500×10^{-3} μm^2, respectively, with thickness ratios of 1/3, 1/2, and 1/6. This core model was designed to simulate the reservoir conditions of Well Block 530 of the Xinjiang Oilfield (Zhang et al., 2026; Zhu et al., 2025a).

2.2. Preparation of CO_2-responsive fluid

Formation water (100 g) was weighed and placed on a magnetic stirrer. With a stirring speed maintained at 500±50 r/min, predetermined masses of reagents A and B were added dropwise in sequence, followed by continuous stirring for 5 min to obtain the prepared CRF solution. The dosage range of reagent A was 0.5%–1.5%, and that of reagent B was 0.1%–0.2%.

For CRF solutions of different pH values, hydrochloric acid and sodium hydroxide solutions were diluted to 1 mol/L. CRF solutions were titrated to target pH values (3, 5, 7, 9, 11, and 13) to obtain CRF solutions with different pH conditions. In addition, for CRF solutions of different salinities, 100 g of deionized water and predetermined masses of sodium chloride were weighed to prepare brine samples with salinities of 0, 5000, 10,000, 12932.5, 15,000, and 20,000 mg/L. Reagents A and B were then added in sequence to prepare CRF solutions with corresponding salinities.

2.3. CRF viscosity measurement

CO_2 at 5 MPa was introduced for 10 min into the reaction vessel containing the CRF solution, as shown in Fig. 2. After the solution had fully reacted with CO_2, the valve was opened slowly. After pressure release, the rotation speed was set to 6 r/min for viscosity measurement by a viscometer (DV-C, Brookfield, USA).

2.4. Infrared spectroscopy testing of CRF

CRF samples (prepared with 1.5% reagent A and 0.2% reagent B) before and after CO_2 reactions were frozen with liquid nitrogen and vacuum-dried for one week. The dried samples were then mixed with potassium bromide and pressed into pellets. Transmittance was measured using a Fourier transform infrared spectrometer (IRTracer-100, Shimadzu, Japan). The instrument resolution was 4 cm^{-1}, the scan range was 400–4000 cm^{-1}, and the number of scans was 16.

2.5. Microstructure characterization of CRF

CRF samples before and after reaction with CO_2 were freeze-dried with liquid nitrogen to form powders. Microstructure characterization was performed using a scanning electron microscope

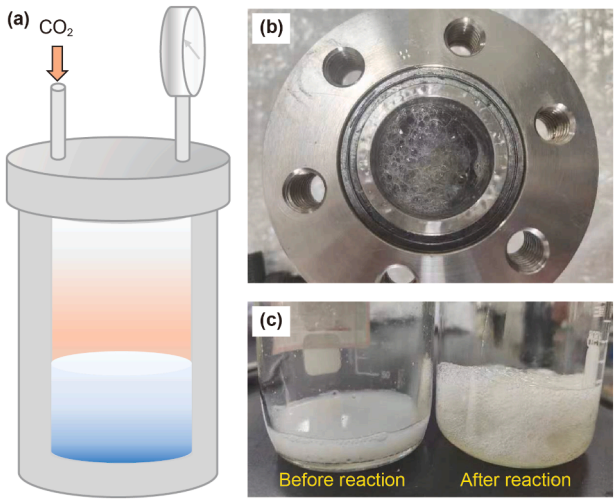

Fig. 2. Schematic diagram of high-temperature and high-pressure reaction device. (**a**) HTHP reaction vessel; (**b**) photograph of the CO_2 responsive fluid (CRF) after reaction with CO_2; (**c**) photographs of the CRF before and after reaction.

(Nova NavoSEM 230, FEI, USA). The magnification ranged from 1000× to 10000× , and the accelerating voltage (HV) was 5.00 kV.

2.6. Thermal stability analysis of CRF

Thermal stability of the freeze-dried CRF samples after reaction with CO_2 was tested using a DSC/TG analyzer (TGA/DSC 3+, Mettler Toledo, Switzerland). The test temperature range was 20–800 °C. The atmosphere was air and the heating temperature range was 30–400 °C. The heating rate was 10 °C/min. The crucible was an alumina crucible.

2.7. Evaluation of conformance control performance of CRF for CO_2-EOR

To investigate the conformance control effect of CRF during CO_2-EOR process in heterogeneous reservoirs, a CRF was prepared using 1.5% reagent A and 0.2% reagent B. A displacement experiment was conducted with an injection rate of 0.1 mL/min. The injected volume of the CRF was 1 pore volume (PV). Three-layer heterogeneous cores with permeabilities of 100/300/1500×10^{-3} μm^2 were used for CO_2 conformance control experiments. The experiment was performed in three stages: primary CO_2 flooding (GF), injection of CRF, and secondary CO_2 flooding (2nd GF). The core was saturated only with water and not with oil, that is, the effect of crude oil was not considered. Pressure variations and gas production rates were recorded in real time to analyze the plugging and CO_2 conformance control performance during the displacement process. The schematic of the experimental setup and procedure is shown in Fig. 3.

To investigate the differences in displacement characteristics of CRF inside cores at the microscopic scale, nuclear magnetic resonance (NMR) analysis of T_2 relaxation spectra was conducted using a SPEC-RC035 instrument (SPEC, Beijing). The NMR T_2 spectrum was selected for analysis rather than the T_1 spectrum. The main reasons are that T_2 testing and analysis are faster, have minimal effect on pore analysis results, and are more commonly used (Zhu et al., 2025a). The experimental parameters were set as follows: pulse interval (TAU) of 100 μs, sampling interval (DW) of 4 μs, number of scans (SCAN) of 32, and signal gain (RG) of 5 dB. Tests covered both the original saturated oil state and core samples after displacement. By analyzing changes in the T_2 relaxation time

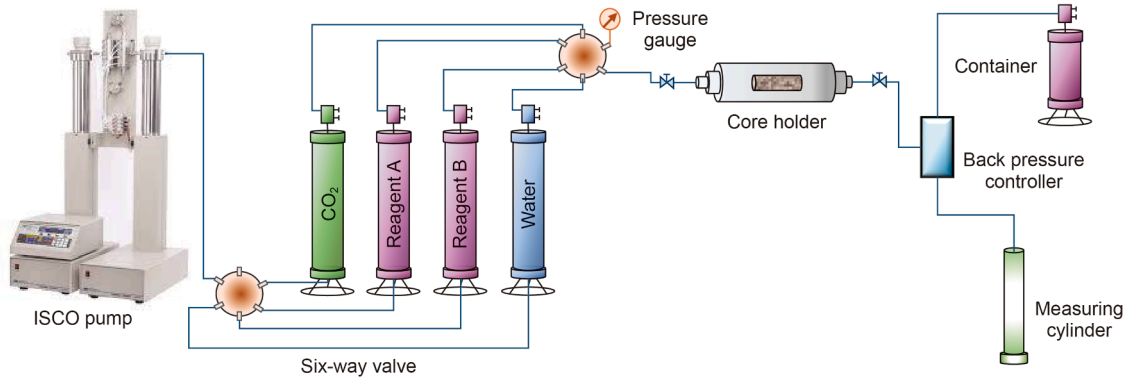

Fig. 3. Schematic of the displacement experimental setup.

distribution, the microscopic oil mobilization effectiveness of the CRF and its CO_2 conformance control characteristics could be quantitatively evaluated.

3. Results and discussion

3.1. Static thickening performance of CRF

After the reaction of the CRF solution with CO_2, micelles could be formed. Structural viscosity was generated, which affected the thickening effect. Under 65 °C (to simulate the target reservoir temperature), CRF solutions were prepared with reagent A at 0.5%–1.5% and reagent B at 0.1%–0.2%. Viscosities of different groups of CRF solutions before and after reaction with CO_2 were measured, as shown in Figs. 4 and 5.

From the curves of viscosity versus concentrations of reagents A and B before reaction with CO_2 in Fig. 4, the initial viscosities of different CRF solutions with different concentration ratios were all in the range of 1.1–1.5 mPa·s. This indicated good injectivity of the CRF before reacting with CO_2. In addition, with increases in concentrations of reagents A and B in the composition of CRF, the viscosity increased slightly. The main reason was that the concentrations of the two surfactants were low, and the molecules could be fully extended in water. Because the concentration of reagent B was very low, weak van der Waals forces were dominant between surfactant molecules.

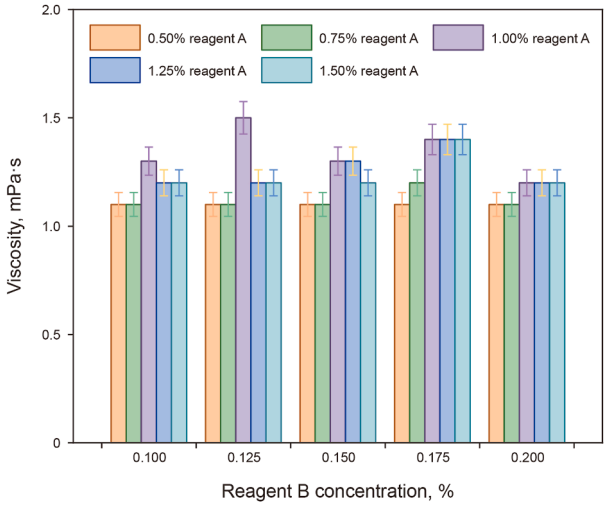

Fig. 4. Variation of solution viscosity with system concentration before reaction with CO_2.

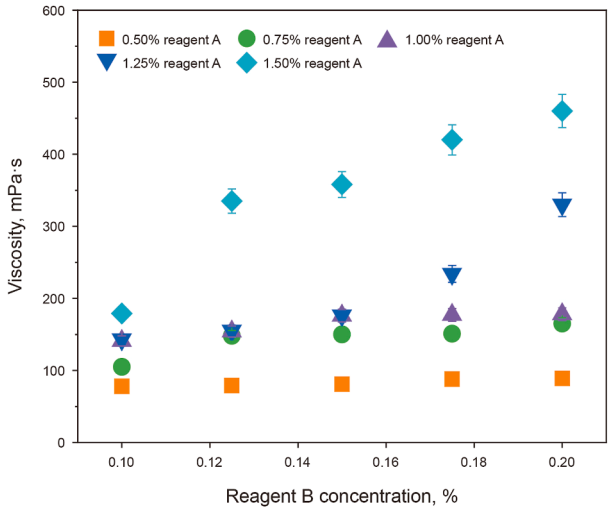

Fig. 5. Cubic-equation fitting plots under different system concentrations.

From Fig. 5, after reaction of the CRF with CO_2, at 0.5% reagent A, the viscosity of the reacted CRF solution increased with the increase in reagent B concentration. The change in the viscosity curve was small, and the viscosity reached 89 mPa·s. This indicated that reagent A in the CRF composition contributed more strongly to CO_2-triggered thickening than reagent B. The main reason was that only when the concentration of reagent A was sufficient could a certain number of worm-like micelles be formed to build a strong network structure. When the concentration of reagent B was fixed, the viscosity of the reacted CRF increased with the increase in reagent A concentration. When the concentration of reagent A was 1.5%, the viscosity growth after reaction increased markedly with the increase in reagent B concentration. The maximum viscosity was measured at 460 mPa·s for the CRF composed of 1.5% reagent A and 0.2% reagent B.

Furthermore, by comparing the viscosities of the CRF before and after reaction, a strong thickening effect was observed. Before exposure to CO_2, the CRF was a spherical micelle solution composed of two surfactants, and the viscosity was low. After reaction with CO_2, bicarbonate formed by dissolved CO_2 protonated the tertiary amine group in reagent A and made it positively charged, as shown in Fig. 6. The micelles transitioned to worm-like structures. The worm-like micelles became entangled and formed

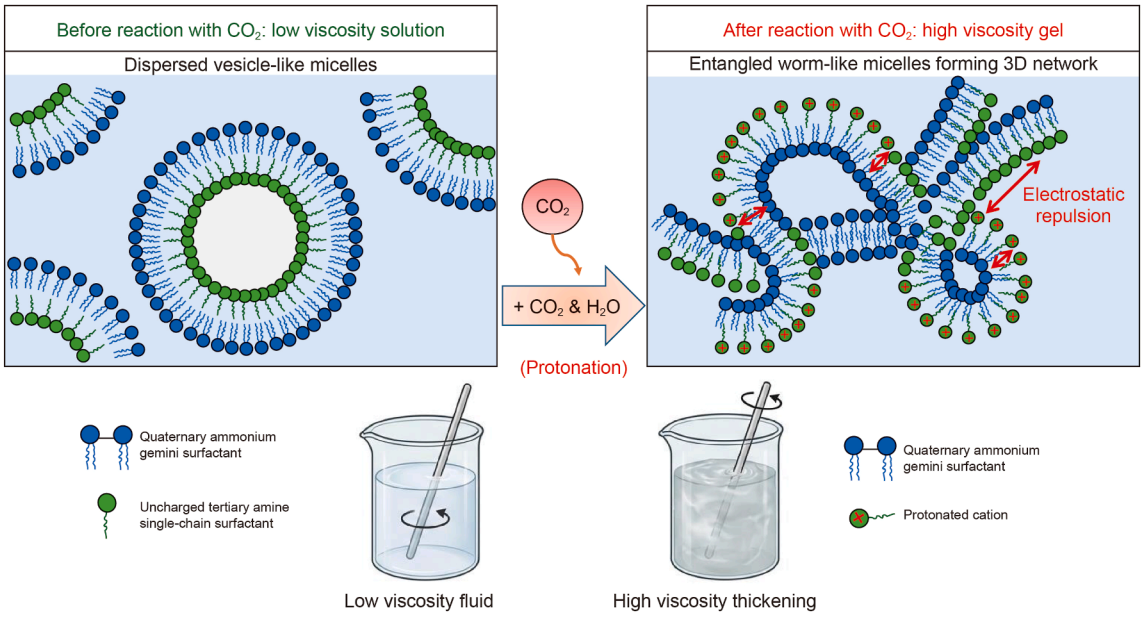

Fig. 6. Chemical reaction of CRF with CO_2 and micelle transformation schematic diagram.

a 3D network. This was manifested as an increase in viscosity of the CRF after reaction with CO_2.

When the CRF was applied to actual reservoir for CO_2 conformance control, a mathematical equation was established to predict the solution viscosity of CRF for different reservoir application requirements.

$$\eta = 1600 C_A^{0.32} C_B^{0.58} \quad (1)$$

where η is the solution viscosity of CRF after reaction with CO_2, mPa·s; C_A and C_B are the concentrations of reagents A and B, %. The Pearson correlation coefficient (Pears) of the equation reached 0.9522.

It was found from the above equation that the viscosity of CRF after reaction with CO_2 exhibited a significant exponential relationship with the concentrations of reagents A and B in the system, with a greater influence from reagent B. As shown in Fig. 5, particularly when the concentration of reagent A exceeded 1.25%, the viscosity of CRF after reaction with CO_2 was most affected by the concentration of reagent B. When the concentration of reagent B reached 0.2%, the viscosity of the system after reaction with CO_2 reached its maximum. Therefore, the optimal formulation of CRF was selected as 1.5% reagent A and 0.2% reagent B.

3.2. Reservoir adaptability analysis of CRF

3.2.1. Effect of reservoir temperature on the thickening performance of CRF

To evaluate the effect of temperature on the thickening performance of the CRF, the solution viscosity after reaction with CO_2 was tested at 25, 45, 65, 85, and 105 °C for the optimal CRF formulation (1.5% reagent A and 0.2% reagent B). The results are shown in Fig. 7.

From Fig. 7, at 25 °C, the solution viscosity of CRF after reaction with CO_2 reached 460 mPa·s. With increasing temperature, the viscosity decreased continuously. The decrease from 25 to 85 °C was small; at 65 °C, the viscosity was 365 mPa·s. When the temperature exceeded 85 °C, the drop in viscosity increased significantly. At 105 °C, the viscosity reached a minimum of 77 mPa·s.

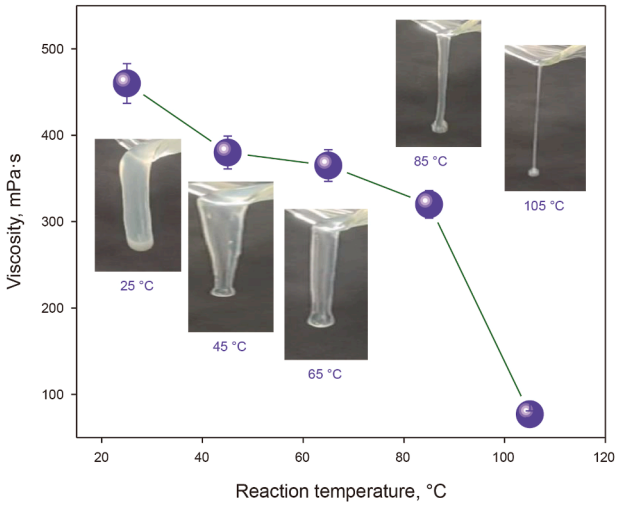

Fig. 7. Viscosity change curves of CRF solutions at different temperatures after reaction with CO_2.

This behavior was attributed mainly to the fact that reagent A (tertiary-amine single-chain surfactant) and reagent B (quaternary ammonium gemini surfactant) were long-chain surfactants. Their long-chain groups were prone to scission at high temperatures, resulting in very weak strength after reaction with CO_2. As the reservoir temperature increased, the solution viscosity of CRF after reaction with CO_2 became lower, mainly because the intermicellar interactions weakened. The stability of the formed structure deteriorated.

Fig. 7 also presents the tongue phenomenon of the solutions after reaction with CO_2 under different temperatures. At 25 °C (ambient), the micellar strength of the CRF solution was the greatest, and the formed tongue width was the widest. With increasing temperature, the micellar strength decreased, the colloidal network weakened, and the tongue width narrowed. At 105 °C, the micellar strength was the smallest, and the tongue phenomenon almost disappeared. Therefore, to obtain a high-

strength responsive material, the suitable temperature range was below 80 °C. Therefore, the CRF was suitable for the reservoir temperature (65 °C) of the CO_2 conformance control process in Block 530, Xinjiang Oilfield.

3.2.2. Effect of formation-water (makeup water) pH on thickening performance of CRF

To evaluate the effect of different formation-water (makeup water) with different pH values on the thickening performance of the CRF, viscosities were tested for the CRF with composition (1.5% reagent A and 0.2% reagent B) at pH values of 3, 5, 7, 9, 11, and 13, before and after reaction with CO_2. The results are shown in Fig. 8.

As shown in Fig. 8, before reaction with CO_2, the CRF at the pH value of 3 exhibited the maximum viscosity, up to 3050 mPa·s. The viscosity decreased as the solution pH value increased. When the pH value increased to 5, the decrease was small. This was mainly because reagent A (tertiary-amine single-chain surfactant) needed acidic conditions for protonation of the tertiary amine (bearing a positive charge) to form wormlike micelles. Therefore, stronger acidity produced more positive charges and led to higher viscosity after reaction. When the pH value increased to 7, the viscosity decreased markedly. When the pH value exceeded 7, little change was measured, and the viscosity was about 2.0 mPa·s.

After reaction with CO_2, the CRF viscosity at the pH value of 3 reached a maximum of 1850 mPa·s. It was mainly because the acidity was weakened after introducing CO_2 (the pH value of water saturated with CO_2 was about 4). Alternatively, other water sources could be used for the preparation of the CRF solution. As the solution pH value increased, the viscosity of the CRF decreased gradually. When the pH value was around 7, the decrease was most obvious. However, when the pH value increased from 7 to 9, the decrease was small. In addition, when the pH value was greater than 9, the viscosity was about 2.0 mPa·s. The reason was that the alkalinity was too strong; even after a short CO_2 purge, acidic conditions could not be achieved, protonation could not occur, wormlike micelles could not be formed. Therefore, the viscosity after reaction showed almost no change. It was noted that acidic solutions should not be selected for solution preparation. In particular, when produced water after CO_2 flooding was used to prepare CRF solutions, the pH value needed to be monitored and adjusted to an appropriate value.

Fig. 8 also showed the tongue-like flow of the solutions after reaction with CO_2 at different pH values. At the pH value of 3, the CRF exhibited the highest viscosity, and the tongue width was the widest. As the pH value increased, the viscosity decreased, and the tongue width narrowed. At the pH value of 9, the viscosity decreased significantly, and the tongue became filament-like. When the pH value exceeded 9, the viscosity was about 2.0 mPa·s, and the tongue appeared water-like. Therefore, to obtain a high-strength CO_2-responsive material, the suitable pH value was around 7. At this pH value, the viscosity before reaction was low, which facilitated injection into the formation; after reaction, the viscosity was higher, which enabled plugging with a certain strength.

3.2.3. Effect of formation-water salinity on the thickening performance of CRF

The effect of different formation-water (makeup water) salinity on the thickening performance of the CRF was evaluated. In this study, the concentration of sodium chloride was used to represent the level of salinity, mainly because the salinity in the Xinjiang Oilfield is relatively low and the content of other ions is minimal (Chen et al., 2023b). The viscosity of the CRF (1.5% reagent A and 0.2% reagent B) after reaction with CO_2 was tested at salinity from 0 to 20,000 mg/L, as shown in Fig. 9.

Before reaction with CO_2, at 0 mg/L salinity, a viscosity of 290 mPa·s was observed for the CRF solution. It was mainly because no ions were present in the solution. The repulsion between micelles was strong (not compressed by other strong electrolytes). Wormlike micelles were easily formed. Thus, a high viscosity was generated. The initial viscosity decreased gradually with increasing salinity. When the salinity reached 5000 mg/L, the viscosity changed little, at about 1.0 mPa·s. Therefore, for this system, the use of fresh water (salinity lower than 5000 mg/L) to prepare the initial solution should have been avoided; otherwise, injection difficulties might have been caused.

After reaction with CO_2, the solution viscosity first increased and then decreased with increasing salinity. When the salinity reached 10,000 mg/L, the maximum viscosity of 527 mPa·s was obtained. It was mainly because, at low salinity, compression of the micellar double layer by Na^+ ions was limited, and greater internal friction was produced, so the viscosity increased. When the salinity reached 20,000 mg/L, the viscosity decreased to a

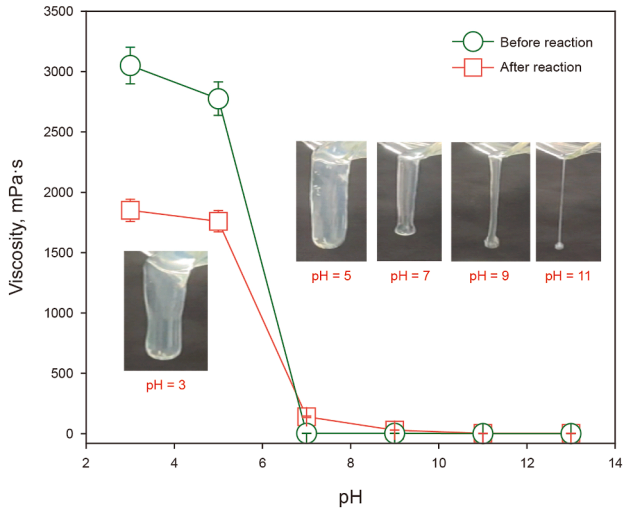

Fig. 8. Viscosity change curves of solutions before and after reaction with CO_2 at different pH values.

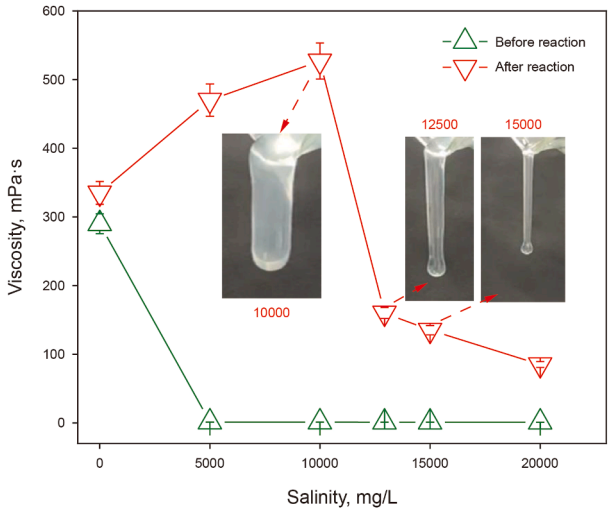

Fig. 9. Viscosity change curves of solutions before and after reaction with CO_2 at different salinity levels.

minimum of 85 mPa·s. At that time, excess Na^+ compressed the micellar double layer, repulsion was significantly weakened, the entanglement of wormlike micelles decreased. Therefore, a significant reduction in viscosity was observed macroscopically.

3.3. Analysis of the thickening mechanism of the CRF

3.3.1. Infrared structural analysis of the CRF

Infrared spectroscopy tests were performed on CRF samples. The characteristic frequency distribution of molecular groups was observed. The main functional groups and absorption peaks of the CRF were analyzed, as shown in Fig. 10.

From Fig. 10, before reaction with CO_2, the main functional groups and absorption peaks of the CRF were as follows. The absorption peak near 3320 cm^{-1} was attributed to N–H stretching vibration. The absorption peak at 2850 cm^{-1} was caused by the antisymmetric stretching vibration of –C–H (methylene). The absorption peak at 2950 cm^{-1} was caused by the symmetric stretching vibration of –C–H (methylene). The absorption peak near 1650 cm^{-1} was caused by –C=O stretching vibration. The characteristic peaks at 1550 and 1460 cm^{-1} were due to the in-plane bending vibration of –N–H. The absorption peak around 1050 cm^{-1} was due to –C–N stretching vibration. The absorption peak near 710 cm^{-1} was caused by the out-of-plane deformation vibration of –N–H.

For the CRF after the addition of CO_2, the main functional groups and absorption peaks were consistent with those of the CRF before reaction. The transmittance of the main absorption peaks decreased. It was because the tertiary amine-based surfactant in the CRF underwent protonation after reaction, which enhanced micellar interactions. Irregular changes in molecular bond vibrations occurred, which affected the shape of the infrared spectrum. These analyses verified from the chemical structure that no new functional groups were formed during the reaction of the CRF with CO_2. Protonation of tertiary amine groups rendered the micelles positively charged, which led to the formation of wormlike micelles. The wormlike micelles intertwined to form a 3D network structure.

3.3.2. Microstructural changes before and after reaction with CO_2

To further verify the thickening mechanism of the CRF (formation of a 3D network structure), a CRF prepared with formation water using 1.5% reagent A and 0.2% reagent B was used. The microstructures of CRF samples before and after reaction with CO_2 are shown in Fig. 11.

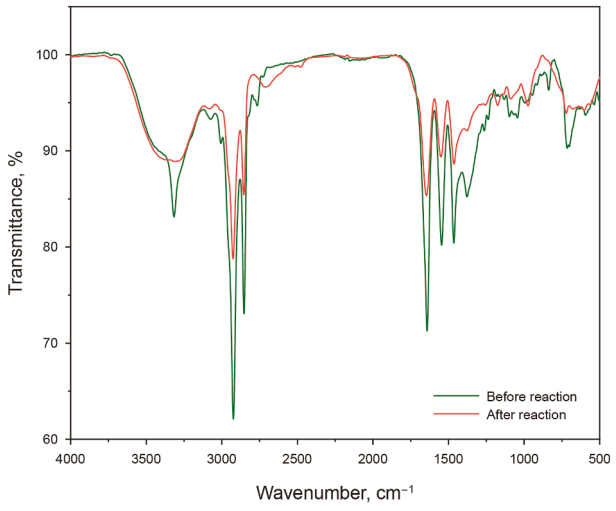

Fig. 10. Infrared spectra of the CRF before and after reaction with CO_2.

As seen in Fig. 11, before reaction with CO_2, the microstructure of the CRF presented an irregular blocky structure. Molecular particles and salt crystals exhibited a stacked lamellar arrangement. The overall structure was loose. It was likely caused by the charge characteristics of the quaternary ammonium salt groups in reagent B of the CRF. It also verified at the microscopic scale, the reason for the low viscosity of the CRF before reaction with CO_2.

After the addition of CO_2, the molecular structure of the solution showed a distinct network structure. It mainly resulted from the protonation of the tertiary amine groups in reagent A, which increased the positive charge of the micelles and led to the formation of wormlike micelles. The wormlike micelles formed high-viscosity aggregates with a 3D structure through van der Waals forces. Fig. 11(c, d) verified the existence of this 3D network structure at the microscopic scale. The mesh size was 10–30 μm, and a relatively dense mesh structure was observed.

3.3.3. Thermal stability analysis of CRF

A CRF prepared in formation water with 1.5 wt% reagent A and 0.2 wt% reagent B was freeze-dried to obtain a powder sample. The thermal stability of the high-viscosity aggregates formed after the CRF reacted with CO_2 was tested, as shown in Fig. 12.

From Fig. 12, it was observed that the mass of the CRF decreased continuously as the temperature increased. The range of 26–200 °C was the first stage of thermal degradation, with a 4% weight loss, which indicated that the CRF remained stable below 200 °C with almost no thermal degradation. The range of 200–300 °C was the second stage, during which most degradation occurred, with a 32% weight loss. The range of 300–510 °C was the third stage, during which minor additional degradation occurred, with an 11% weight loss. This indicated that the molecular structure of the CRF had good thermal stability in the range of 0–200 °C. The heat-flow curve first decreased, then increased, and then decreased again. An exothermic event was observed at 0–50 °C, possibly due to solute crystallization of the CRF. The heat-flow curve rose at 50–100 °C with an endothermic peak, possibly a low-temperature melting peak caused by incomplete solute crystallization. An exothermic peak appeared at 100–150 °C, possibly due to secondary crystallization of the solute. An endothermic peak appeared at 150–420 °C, possibly due to the melting of the solute. Therefore, when the temperature exceeded 100 °C, changes in the chemical structure of the CRF occurred, which affected its responsive properties. Macroscopically, the viscosity after reaction with CO_2 decreased significantly when the temperature exceeded 100 °C (see Fig. 7). Therefore, when the CRF was employed to reservoir development, the application was suitable for reservoirs below 100 °C. When the reservoir temperature was below 50 °C, better performance was achieved.

3.4. Analysis of the conformance control effect of CRF in CO_2 flooding

During oilfield CO_2 flooding processes, reservoir heterogeneity was one of the primary causes of gas channeling. To evaluate the CO_2 conformance control performance of CRF in heterogeneous reservoirs during CO_2 flooding, laboratory displacement experiments in heterogeneous cores were conducted. A CRF formulated with 1.5% reagent A and 0.2% reagent B was injected into three-layer heterogeneous cores for gas channeling plugging tests. Fig. 13 illustrates the dynamic changes of pressure difference and gas production rate during the displacement process.

According to Fig. 13, under heterogeneous conditions, the injection pressure difference during water flooding and primary CO_2

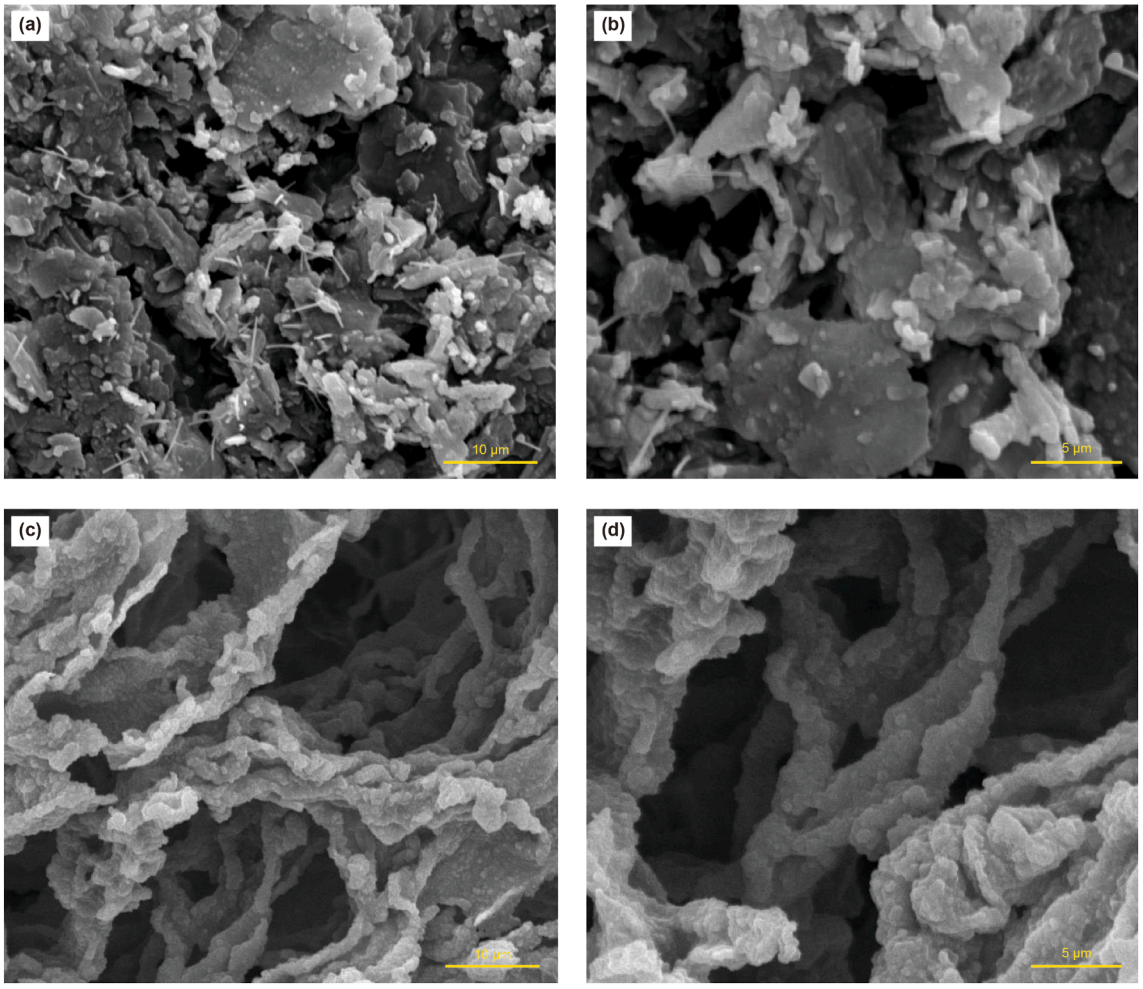

Fig. 11. SEM images of the CRF. Before reaction with CO_2, magnified 5000 (**a**) and 10,000 (**b**) times; after reaction with CO_2, magnified 5000 (**c**) and 10,000 (**d**) times.

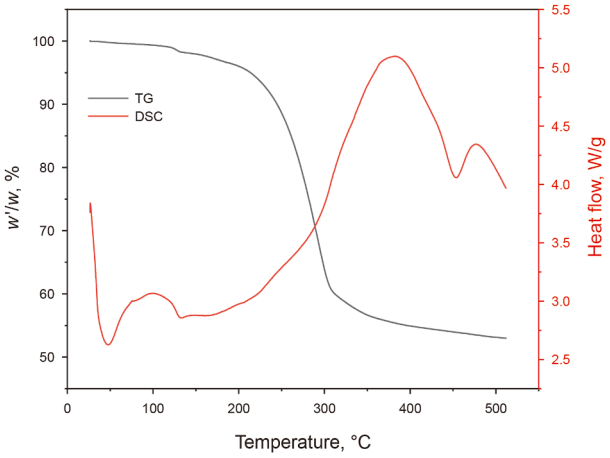

Fig. 12. TG-DSC plots of the CRF.

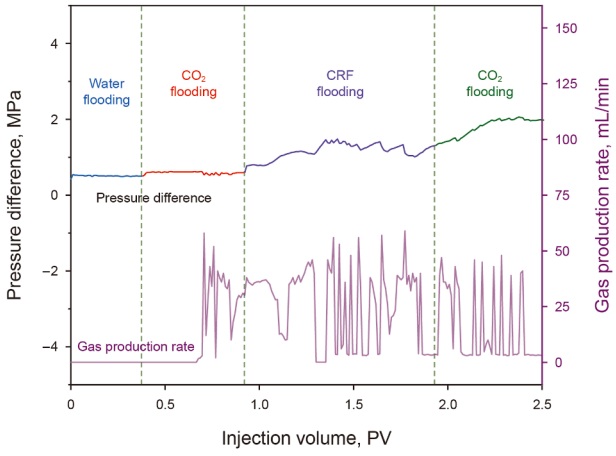

Fig. 13. Core displacement process of CO_2 flooding with CRF treatment.

flooding exhibited small variations. When the CRF was injected, the pressure gradually increased, showing an upward trend with more significant fluctuations. After complete gas channeling occurred, the injection pressure difference tended to stabilize.

After injection of the CRF followed by secondary CO_2 flooding, the pressure difference increased to 0.85 MPa, with a pressure gradient of 0.27 MPa/cm. The gas breakthrough time during the secondary CO_2 injection stage was 0.38 PV, and the plugging efficiency at breakthrough was 70%. Thus, during the CRF injection stage in heterogeneous cores, the injection climbing pressure was not high. The plugging efficiency at gas breakthrough was approximately 70%, indicating a good injectivity of the system.

This suggested that the system effectively extended gas breakthrough time and exhibited good CO_2 conformance control performance.

To further investigate the microscopic CO_2 conformance control effect of CRF in heterogeneous cores, nuclear magnetic resonance (NMR) T_2 tests were performed on the cores at different displacement stages. Fig. 14 compares T_2 spectra after water flooding, primary CO_2 flooding, and secondary CO_2 flooding. Fig. 15 presents comparisons of peak areas of small pores, medium pores, and large pores in T_2 spectra at different displacement stages. In Fig. 14, three regions are shown in the T_2 peaks. In this study, peaks below 1 ms were defined as small pores, peaks among 1–10 ms were defined as medium pores, and peaks above 10 ms were defined as large pores.

As shown in Fig. 15, in the heterogeneous core with permeabilities of 100/300/1500 $\times$ 10^{-3} μm^2, after secondary CO_2 flooding compared with primary CO_2 flooding, the peak area of small pores (below 1 ms) increased from 22.44 to 65.68, an increase of 43.24. The peak areas of medium and large pores (above 1 ms) decreased from 17371.64 to 3692.39, a reduction of 13679.25. Therefore, after secondary CO_2 flooding in the heterogeneous core, an increase in the peak area of small pores and a decrease in the peak areas of medium and large pores were observed. This indicated that the CRF provided good CO_2 conformance control in medium- and high-permeability zones and further enhanced plugging in large pore spaces. The mechanism was similar to other plugging materials used for improving CO_2 flooding conformance, mainly by further plugging high-permeability channels and enhancing CO_2 displacement efficiency in large pores. Conformance control (or mobilization) in small pores might require modification of the CO_2–formation fluid properties, such as pressurization to enhance CO_2 diffusion and mass transfer (Zhu, 2023).

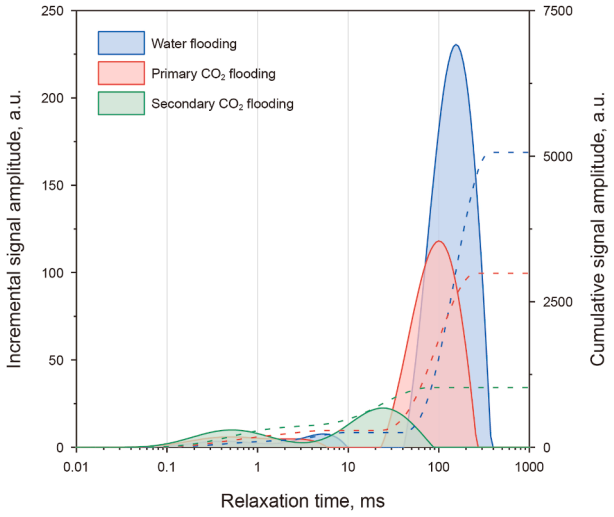

Fig. 14. Changes in T_2 spectra of the heterogeneous core at different stages.

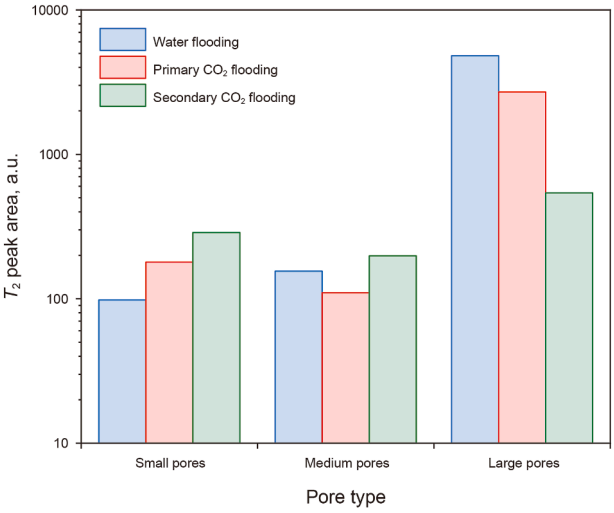

Fig. 15. Comparison of T_2 spectral peak areas of the heterogeneous core at different displacement stages.

4. Conclusions

The thickening performance of the CO_2 responsive fluid (CRF) and its influencing factors were systematically analyzed in this study. Combined with displacement experiments and NMR technology, the CO_2 conformance control mechanism of CRF in heterogeneous cores was revealed. The main conclusions were as follows.

(1) The concentrations of reagents A and B affected the viscosity of CRF solution. The maximum viscosity of 460 mPa·s was obtained when CRF was prepared with 1.5% reagent A and 0.2% reagent B.
(2) CRF exhibited good thickening performance under medium- and high-temperature conditions. At 105 °C, the minimum solution viscosity reached 77 mPa·s. Below 80 °C, CRF showed excellent viscosity enhancement, mainly due to the stability of its chemical structure.
(3) CRF demonstrated good thickening performance under low to medium salinity conditions (0–10,000 mg/L). At a salinity of 10,000 mg/L, the maximum viscosity reached 527 mPa·s. High salinity compressed the double layer of worm-like micelles and reduced their entanglement effect.
(4) When the pH value of the make-up water was 7, CRF presented the best thickening performance. Excessively low pH value caused injectivity issues, while excessively high pH value inhibited the formation of worm-like micelles.
(5) SEM and TG/DSC tests confirmed that the CRF structure exhibited sheet-like surfaces before reacting with CO_2. It transformed into an obvious 3D network structure after reaction. Below 100 °C, the chemical structure displayed good thermal stability.
(6) A static thickening mathematical equation of CRF was established to predict viscosity variation, enabling rapid screening under different reservoir conditions.
(7) Core displacement tests and NMR T_2 spectral analysis indicated that CRF exhibited good plugging and CO_2 conformance control in heterogeneous formations. The gas breakthrough time was extended to 0.38 PV, improving the CO_2 flooding performance.

CRediT authorship contribution statement

Xiao-Guang Wang: Writing – original draft, Validation, Investigation, Data curation. **De-Hua Liu:** Validation, Supervision, Methodology, Investigation. **Hong-Bin Cheng:** Writing – original draft, Validation, Investigation. **Qiang Luo:** Validation, Investigation. **Ke Tang:** Validation, Investigation. **Dao-Yi Zhu:** Writing –

review & editing, Writing – original draft, Validation, Supervision, Methodology, Data curation, Conceptualization.

Declaration of competing interest

The authors declare that they have no known competing financial interests or personal relationships that could have appeared to influence the work reported in this paper.

References

Afolabi, F., Dzulkarnain, I., Kwon, S., Martyushev, D.A., Lee, J.H., Jufar, S.R., Al-Akbari, F., 2025. Gels for CO_2 geo-storage and conformance control: A systemic review of behavior and performance. Deep Undergr. Sci. Eng. 4 (4), 612–637. https://doi.org/10.1002/dug2.70027.

Bai, L., Gao, Y., Yang, S., Zhao, Y., Du, J., Luan, H., Tang, K., Yue, J., Zhu, D., 2025. Nanosheet-reinforced CO_2 foam systems for CO_2 conformance control: Effects of reservoir permeability and heterogeneity. Energy Fuels 39 (37), 17834–17844. https://doi.org/10.1021/acs.energyfuels.5c03934.

Chen, P., Bose, S., Selveindran, A., Thakur, G., 2023a. Application of CCUS in India: Designing a CO_2 EOR and storage pilot in a mature field. Int. J. Greenh. Gas Control 124, 103858. https://doi.org/10.1016/j.ijggc.2023.103858.

Chen, S., Li, J., Chen, S., Qin, J., Wang, G., Yi, Y., Zhang, L., Wang, R., Zhu, D., 2023b. Experimental evaluation of combined plugging system for CO_2-improved oil recovery and storage. Energy Fuels 37 (6), 4401–4412. https://doi.org/10.1021/acs.energyfuels.3c00246.

Chen, Z., Zhou, Y., Li, H., 2022. A review of phase behavior mechanisms of CO_2 EOR and storage in subsurface formations. Ind. Eng. Chem. Res. 61 (29), 10298–10318. https://doi.org/10.1021/acs.iecr.2c00204.

Deng, J.N., Zhao, H., Zheng, H., Zhuang, Y., Wei, K., Yuan, H., Deng, Z., Gao, Y., Zhou, X., Yu, T., Hu, H., Lu, G., Zhang, X., 2025. CO_2-responsive preformed particle gels with high strength for CO_2 conformance control in heterogeneous reservoirs. Fuel 379, 133040. https://doi.org/10.1016/j.fuel.2024.133040.

Fang, P., Yang, Z., Zhang, Q., Yu, H., Feng, F., Wan, Y., Wei, J., Mei, Y., Cao, M., 2025a. Chemically enhanced water-alternating-gas injection for improved CO_2 sweep efficiency and geological sequestration in CO_2-EOR: Insights from physical experiments and molecular simulation. Results Eng., 106239 https://doi.org/10.1016/j.rineng.2025.106239.

Fang, P., Zhang, Q., Wu, M., Zhou, C., Yang, Z., Yu, H., Ji, Z., Yi, L., Jiang, W., Chen, X., Gao, Y., Zhou, M., Cao, M., 2025b. An intelligent CO_2-responsive hydrogel for applications in enhanced oil recovery and CO_2 geological storage. Sep. Purif. Technol. 359, 130526. https://doi.org/10.1016/j.seppur.2024.130526.

Fu, L., Gong, J., Liu, Q., Ma, Q., Shao, M., Liao, K., Chang, A., Zhu, T., Ren, Z., Wang, T., 2025. Synthesis and evaluation of CO_2 responsive surfactants based on dynamic imine bond. Colloids Surf. A Physicochem. Eng. Asp. 706, 135820. https://doi.org/10.1016/j.colsurfa.2024.135820.

Gao, Q., Wang, B., Trivedi, J., Xu, X., Liu, S., 2024. Experimental investigations and MD simulation on nanoparticle-enhanced CO_2-responsive foam (NECRF): Implications on CO_2-EOR. ACS Appl. Mater. Interfaces 16 (33), 43647–43660. https://doi.org/10.1021/acsami.4c09052.

Huang, T., Cheng, L., Cao, R., Wang, X., Jia, P., Cao, C., 2024a. Molecular simulation of the dynamic distribution of complex oil components in shale nanopores during CO_2-EOR. Chem. Eng. J. 479, 147743. https://doi.org/10.1016/j.cej.2023.147743.

Huang, X., Zhang, M., Su, X., Feng, Y., 2024b. CO_2-responsive polymer promoted by polyether to efficient viscosity increase for CO_2 plugging. Polymer 306, 127227. https://doi.org/10.1016/j.polymer.2024.127227.

Li, Z., Liu, J., Su, Y., Fan, L., Hao, Y., Kanjibayi, B., Huang, L., Ren, S., Sun, Y., Liu, R., 2023. Influences of diffusion and advection on dynamic oil-CO_2 mixing during CO_2 EOR and storage process: Experimental study and numerical modeling at pore-scales. Energy 267, 126567. https://doi.org/10.1016/j.energy.2022.126567.

Luo, Y., Tang, X., Li, Z., Zhou, C., Li, R., Fu, S., 2025. Ultra-stable and switchable foams enabled by a rigid bio-based pH-responsive gemini surfactant. J. Surfactants Deterg. 29 (2), 197–207. https://doi.org/10.1002/jsde.70005.

Lv, Q., Zheng, R., Zhou, T., Guo, X., Wang, W., Li, J., Liu, Z., 2022. Visualization study of CO_2-EOR in carbonate reservoirs using 2.5D heterogeneous micromodels for CCUS. Fuel 330, 125533. https://doi.org/10.1016/j.fuel.2022.125533.

Shen, H., Yang, Z., Li, X., Peng, Y., Lin, M., Zhang, J., Dong, Z., 2021. CO_2-responsive agent for restraining gas channeling during CO_2 flooding in low permeability reservoirs. Fuel 292, 120306. https://doi.org/10.1016/j.fuel.2021.120306.

Su, X., Cunningham, M.F., Jessop, P.G., 2013. Switchable viscosity triggered by CO_2 using smart worm-like micelles. Chem. Commun. 49 (26), 2655–2657. https://doi.org/10.1039/C3CC37816K.

Sun, X., Bai, B., Alhuraishawy, A.K., Zhu, D., 2021. Understanding the plugging performance of HPAM-Cr (III) polymer gel for CO_2 conformance control. SPE J. 26 (5), 3109–3118. https://doi.org/10.2118/204229-PA.

Wang, Y.-Y., Wang, X.-G., Dong, R.-C., Teng, W.-C., Zhan, S.-Y., Zeng, G.-Y., Jia, C.-Q., 2023. Reservoir heterogeneity controls of CO_2-EOR and storage potentials in residual oil zones: Insights from numerical simulations. Pet. Sci. 20 (5), 2879–2891. https://doi.org/10.1016/j.petsci.2023.03.023.

Wang, Z., Bai, B., Long, Y., Wang, L., 2019. An investigation of CO_2-responsive preformed particle gel for conformance control of CO_2 flooding in reservoirs with fractures or fracture-like channels. SPE J. 24 (5), 2398–2408. https://doi.org/10.2118/197046-PA.

Wu, K., Zhang, J., Feng, Q., Wang, S., Wu, Z., Shang, L., Gao, X., 2025. Co-optimization of well schedule and conformance control parameters assisted with transformer-LSTM for CO_2-EOR and storage in oil reservoirs. Energy, 136891. https://doi.org/10.1016/j.energy.2025.136891.

Yan, W., Li, Z., Peng, H., Chen, Y., Hao, Y., Guo, F., Xiang, H., Liu, K., Xu, X., Xiao, R., 2026. Feasibility evaluation of CO_2-EOR and storage in low oil saturation reservoir. Fuel 411, 138029. https://doi.org/10.1016/j.fuel.2025.138029.

Zhang, J., Tan, H.-G., Zhang, T., Gao, Y.-Q., Cheng, H.-B., Li, H.-Y., Zhu, D.-Y., 2026. New injection method using composite gel system and gel breaker to improve sweep efficiency and mitigate formation damage. Pet. Sci. 23 (1), 383–392. https://doi.org/10.1016/j.petsci.2025.10.016.

Zhang, L., Li, C., Zhang, Y., Wang, X., Yao, X., Sun, Y., Li, F., Yang, H., 2024. CO_2-EOR and storage in a low-permeability oil reservoir: Optimization of CO_2 balanced displacement from lab experiment to numerical simulation. Geoenergy Sci. Eng. 243, 213325. https://doi.org/10.1016/j.geoen.2024.213325.

Zhao, Y., Rui, Z.-H., Zhang, Z., Chen, S.-W., Yang, R.-F., Du, K., Dindoruk, B., Yang, T., Stenby, E.H., Wilson, M.A., 2022. Importance of conformance control in reinforcing synergy of CO_2 EOR and sequestration. Pet. Sci. 19 (6), 3088–3106. https://doi.org/10.1016/j.petsci.2022.09.036.

Zhou, J., Deissenroth-Uhrig, M., Gallei, M., 2025. Advances in stimuli-responsive organic materials and polymers toward intelligent CO_2 capture. Adv. Funct. Mater. 36 (9), e20959. https://doi.org/10.1002/adfm.202520959.

Zhu, D., 2023. CO_2 and Geo-Energy Engineering. China Petrochemical Press (in Chinese).

Zhu, D., Peng, S., Zhao, S., Wei, M., Bai, B., 2021. Comprehensive review of sealant materials for leakage remediation technology in geological CO_2 capture and storage process. Energy Fuels 35 (6), 4711–4742. https://doi.org/10.1021/acs.energyfuels.0c04416.

Zhu, D.-Y., Zhang, J., Zhang, T., Gao, Y.-Q., Guo, S., Yang, Y.-L., Lu, J.-M., 2025a. Damage mechanism analysis of polymer gel to petroleum reservoirs and development of new protective methods based on NMR technique. Pet. Sci. 22 (3), 1225–1233. https://doi.org/10.1016/j.petsci.2024.12.004.

Zhu, D., Lu, J., Zhang, J., Gao, Y., Guo, S., Yang, Y., Zhang, T., Tan, H., 2025b. N_2 and CO_2 nanobubble enhanced oil recovery in conglomerate reservoirs based on NMR technology. Energy Fuels 39 (28), 13378–13385. https://doi.org/10.1021/acs.energyfuels.5c02717.

Zhu, D., Zhao, Q., Zhang, J., Gao, Y., Li, G., Wu, Z., 2025c. New insight of CO_2 corrosion performance on cement for enhanced oil recovery and carbon geological storage based on nuclear magnetic resonance technology. Energy Fuels 39 (7), 3396–3406. https://doi.org/10.1021/acs.energyfuels.4c04825.

Zhu, D., Yang, Y., Tan, H., Guo, S., Lu, J., Zhang, T., Zhang, J., Gao, Y., Li, H., Cheng, H., 2026. CO_2 conformance control and carbon storage performance of particle gels in fractured reservoirs using nuclear magnetic resonance methods. SPE J. 31 (1), 588–601. https://doi.org/10.2118/231408-PA.

Zhu, Z., Song, Y., Gao, Q., Wang, C., 2023. The application of CO_2-responsive materials on enhanced oil recovery for fractured tight oil reservoirs. Front. in Earth Sci. 10, 1053307. https://doi.org/10.3389/feart.2022.1053307.